

Nonlinearity in a medical ultrasound probe under high excitation voltage

Thong Huynh¹, Geir Ultveit Haugen², Trym Eggen², Lars Hoff¹

¹Department of Microsystems, University of South-Eastern Norway, Horten, Norway

²GE Vingmed Ultrasound AS, Horten, Norway

Huynh, T., Haugen, G. U., Eggen, T. & Hoff, L. (2021). Nonlinearity in a Medical Ultrasound Probe Under High Excitation Voltage. *IEEE Transactions on Ultrasonics, Ferroelectrics, and Frequency Control*, 68(3), 784-795.
<https://doi.org/10.1109/TUFFC.2020.3021981>

© 2021 IEEE. Personal use of this material is permitted.

Permission from IEEE must be obtained for all other uses, in any current or future media, including reprinting/republishing this material for advertising or promotional purposes, creating new collective works, for resale or redistribution to servers or lists, or reuse of any copyrighted component of this work in other works.

Nonlinearity in a medical ultrasound probe under high excitation voltage

Thong Huynh¹, Geir Ultveit Haugen², Trym Eggen², Lars Hoff¹

¹Department of Microsystems, University of South-Eastern Norway, Horten, Norway

²GE Vingmed Ultrasound AS, Horten, Norway

Abstract—Tissue harmonic imaging is often the preferred ultrasound imaging modality due to its ability to suppress reverberations. The method requires good control of the transmit stage of the ultrasound scanner, as harmonics in the transmitted ultrasound pulses will interfere with the harmonics generated in the tissue during nonlinear propagation, degrading image quality. In this study, a medical ultrasound probe used in tissue harmonic imaging was experimentally characterized for transmitted 2nd harmonic distortion to identify and compare sources of nonlinear distortion in the probe and transmit electronics. The system was tested up to amplitudes above what is found during conventional operation, pushing the system to the limits in order to investigate the phenomenon. Under these conditions, 2nd harmonic levels up to -20 dB relative to the fundamental frequency were found in the ultrasound pulses transmitted from the probe. The transmit stage consists of high-voltage transmit electronics, cable, tuning inductors, and the acoustic stack. The contribution from the different stages in the ultrasound transmit chain was quantified by separating and measuring at different positions. Nonlinearities in the acoustic transducer stack were identified as the dominating source for 2nd harmonics in the transmitted ultrasound pulses. Contribution from other components, e.g. transmit electronics and cable and tuning circuitry, were found to be negligible compared to that from the acoustic stack. Investigation of the stack's electrical impedance at different driving voltages revealed that the impedance changes significantly as function of excitation voltage. The 2nd harmonic peak in the transmitted pulses can be explained by this nonlinear electrical impedance distorting the driving voltage and current.

Index Terms—tissue harmonic imaging, nonlinearity, ultrasound transducer, piezoelectric

I. INTRODUCTION

The principle of tissue harmonic imaging is transmitting an ultrasound pulse at one frequency and receiving echoes at harmonics of this frequency, usually the 2nd harmonic, generated from nonlinear sound propagation in the tissue [1]–[4]. Tissue harmonic imaging has been shown to give advantages over conventional imaging methods in terms of reduced clutter and reverberation artifacts and improved feature delineation. Clinical endocardial studies have shown that in some patients, features that were not shown in conventional ultrasound images were visible using 2nd harmonic imaging [5].

However, the method is vulnerable to undesired 2nd harmonics generated in the transmit stage of the ultrasound scanner. These will interfere with the 2nd harmonics generated in the tissue, which are usually more than 20 dB below the fundamental [1], [6]. To achieve successful imaging, the level of transmitted 2nd harmonics should be sufficiently suppressed compared to this level.

Second harmonics in the transmitted ultrasound pulse come from nonlinear distortion in the transmit chain of the ultra-

sound scanner, and will normally increase with increasing transmit power. The transmit chain consists of several sub-systems, and the source of this nonlinear distortion may be one dominant sub-system, or a combination of several parts in the system. This study investigated the distortion in each part of the transmit chain of a clinical ultrasound probe, quantifying the various sources of transmitted 2nd harmonics. Electrical signals were measured at different positions in the transmit chain, acoustic pulses were measured with a hydrophone, some components were replaced, and measurements were done at varying driving voltage amplitudes, enabling us to identify and quantify the sources of nonlinear distortion in the system. The primary aim of this paper was not to minimize the transmitted second harmonic, but rather to provide a reliable set of measurements identifying its sources and quantifying the level, thereby providing useful information when developing techniques to avoid or compensate for the effects, if deemed necessary. Previous work [7] has introduced an empirical method for compensating the 2nd harmonic distortion. This method showed good suppression of transmitted 2nd harmonics, but it is time consuming and does not provide any insight into the mechanism causing the 2nd harmonic distortion. Better understanding of the causes for nonlinearities the transmit chain could help improve suppression of the transmitted harmonics, e.g. by identifying and compensating for the main source for nonlinear distortion.

The transmit chain of a scanner can be divided into two main parts, the electronic circuit, comprising electrical excitation sources and tuning, and the electro-acoustic transducer, converting between electrical signals and mechanical vibrations. Nonlinearities in the electronic part can be related to a nonlinear voltage-current characteristic of electronic components in the circuit. Typically, such nonlinearities increase with voltage and current, but there are exceptions to this, e.g. diodes behave nonlinearly at low voltages. Nonlinearities in the transducer may relate to its structural design, such as the emerging micromachined CMUT and PMUT technologies resulting in transducers that are nonlinear by design. The inherent nonlinearity in CMUTs can be attributed to the electrostatic force being proportional to the square of the applied voltage [8], while PMUTs utilize a nonlinear bending of the transducer membrane [9]. Contrary to this, piezoelectric transducers operating in bulk-mode are usually assumed to be linear. However, this is an approximation, and a nonlinear response may be seen when driving the transducers at high power. This nonlinearity may originate from both mechanical, piezoelectric and electric behaviour of the materials used.

Most transducers in current clinical ultrasound scanners are designed as piezoelectric arrays operating in bulk mode.

Each element in the array is an acoustic stack consisting of an active piezoelectric layer, backing, and one or more acoustic matching layers. In addition, there is bonding material between the layers, filler material between the array elements, and an acoustic lens in front of the stack. The piezoelectric material in the active layer may behave nonlinearly at high voltage excitation, introducing both dielectric, mechanical and piezoelectric non-linear effects [10]. One manifestation of nonlinearity in a piezoelectric material is the variation of the impedance spectrum with increasing strain levels. Perez and Albareda reported how impedances of 3 thin disk piezoelectric samples (PXE-5, PZT-4, PZT-8) vary at different mechanical strain levels, near resonance [11]. Sebald et al. observed similar phenomena in relaxor single crystals, studying PMN-PT and PZN-PT lateral resonance bars [12]. Models for this nonlinear impedance have been proposed, e.g. by adding a third order coefficient for mechanic stress and viscous losses to the nonlinear constitutive equations [12] or adding nonlinear components to the equivalent circuit of the structure [13], [14]. Values for the nonlinear parameters in these models were found by fitting simulations to experimental measurements. Another exhibition of nonlinearity in the piezoelectric material is the 2nd harmonic generation, which has been observed in displacement and particle velocity measurements for different ceramic piezoelectric materials working in both 3-1 and 3-3 modes at the resonance frequency [15], [16]. For the passive materials used in the backing and matching layers, a nonlinear stress-strain relationship may become important at large strains, generating 2nd harmonics in these layers as well.

Nonlinearity in electrical components is known, and several studies have investigated nonlinearity in piezoelectric materials also. But to our knowledge, there is no literature available investigating and comparing the contribution of these non-linear sources to the 2nd harmonic distortion in a complete ultrasound imaging system. This study aims to fill this gap by first quantifying the 2nd harmonic level transmitted by a clinical ultrasound scanner and then identifying and comparing the sources for the distortion. This will provide information to help designers further optimize the transmit pulses used in tissue harmonic imaging, thereby contributing to improved image quality. The 2nd harmonic level in ultrasound pulses from a medical probe was first measured in a water tank using a hydrophone. The sources for the observed 2nd harmonic generation were then sought by measuring electrical signals at various positions in the transmit chain, under varying experimental conditions, and after replacing selected components. Our results indicate that the main source for 2nd harmonics in the transmitted ultrasound pulses is the acoustical transducer stack

II. METHODS

A. Measurement of 2nd harmonic in transmitted ultrasound pulses

Transmitted pulses from a medical ultrasound probe were measured by a hydrophone in a water tank (AIMS III Scanning Tank, Onda Corporation, USA). A schematic drawing of the setup is shown in Fig. 1. The probe comprises a cardiac phased

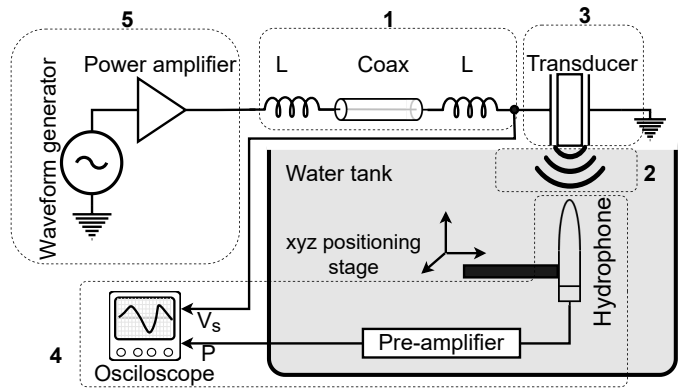


Fig. 1. Schematic illustration of the set up to measure ultrasound pulses from a clinical probe. The measurements were done in a water tank using a calibrated hydrophone. The waveform generator and power amplifier can be replaced by the 3-level pulser mode in an ultrasound scanner. 5 possible nonlinear sources were marked.

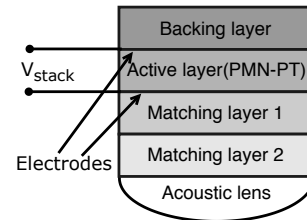


Fig. 2. Structure of one transducer element in the probe. The acoustic lens is focused in the elevation direction.

array transducer with cable assembly containing an electrical tuning network for each element. In most of the measurements reported in this study, only one element in the probe was used. The probe was designed for adult cardiac imaging, working in the frequency range between 1.4 and 4.6 MHz. For 2nd harmonic imaging, the lower end of the transducer bandwidth is used when transmitting, while echoes at twice the transmit frequency are received using the upper part of the bandwidth. In this paper, the transmit frequency was 2 MHz, giving a 2nd harmonic at 4 MHz. The transducer stack comprised an active layer of the ferroelectric single crystal $\text{Pb}(\text{Mg}_{1/3}\text{Nb}_{2/3})\text{O}_3\text{-PbTiO}_3$ (PMN-PT), backing, matching layers, and an outer acoustic lens. This is referred to as the acoustic stack, and is illustrated schematically in Fig. 2. The piezoelectric in the stack was designed to work in beam mode [17], i.e. the working strain is parallel to the poling direction and electric field. Typical values for piezoelectric material parameters in this material are given in [18]. The stack is connected to the transmit electronics by a shielded 2 meter long coaxial cable. Each end of the cable contains a tuning inductor to optimize the electric energy transfer to the transducer.

Two different transmitters were used to excite the ultrasound probe in this analysis. One was the 3-level pulser inside a clinical ultrasound scanner, generating square-wave pulses. Alternatively, to better control the details of the output pulses, a 14-bit arbitrary waveform generator was used (PicoScope 5244B, Pico Technology), connected to a power amplifier (E&I 2100L, Electronics & Innovation, Ltd). The signal gen-

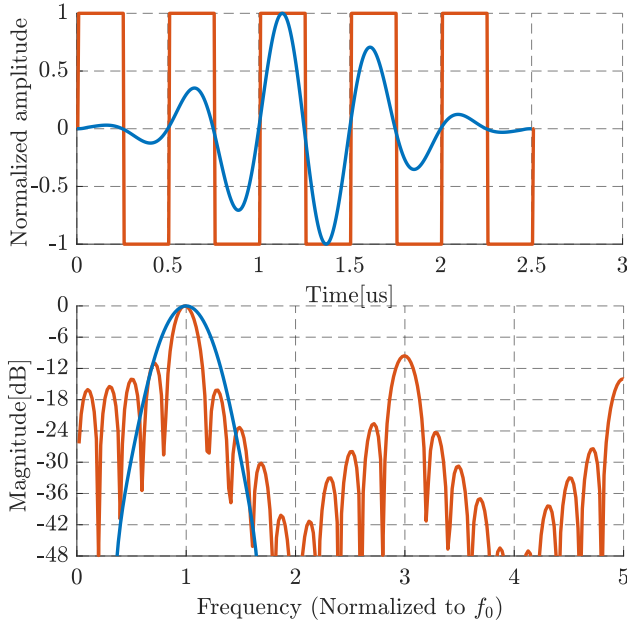


Fig. 3. Definitions of the two excitation waveforms used to excite the transducer, and their power spectra. The 5-cycle square-wave (red) was programmed in the clinical scanner, while the 5-cycle Gaussian enveloped sine-wave (blue) was programmed in the arbitrary waveform generator.

erator was programmed to deliver Gaussian enveloped sine-wave pulses. The bipolar waveforms from the scanner had notches at the even harmonic frequencies, but the spectral side lobes and odd harmonics were high. The Gaussian pulses from the signal generator and power amplifier suppressed all harmonics to below the dynamic range of the system. For both transmitters, the amplitude of the driving voltage was varied from 5 V to 80 V, either by programming the output voltage of the waveform generator or by defining the transmit voltage in the clinical scanner. In the following, this nominal voltage is denoted V_{in} , while the actual voltage measured across the acoustic stack is denoted V_s .

The excitation pulse length was 5 cycles. This is longer than typical imaging pulses, and was chosen because the narrower bandwidth makes it easier to isolate and quantify the 2nd harmonic. The two different excitation waveforms used and their power spectra are shown in Fig. 3. The square-wave is from the clinical scanner, and the Gaussian-enveloped sine-wave is from the arbitrary function generator. The figure shows the pulse shapes programmed into the generators, the actual voltage pulses will deviate from this due to limited bandwidth and frequency dependent loading.

Acoustic pulses were measured using a calibrated hydrophone (HGL-0200, Onda Corporation) with a preamplifier (AG-2010, Onda Corporation) connected to a digital oscilloscope (PicoScope 5244B). The oscilloscope was configured at 12-bit resolution, and the input range was scaled automatically to fit the actual input signal. This provides a sufficient dynamic range for resolving the 2nd harmonic in the transmit pulse, i.e. 20 to 30 dB lower than the fundamental. The measured

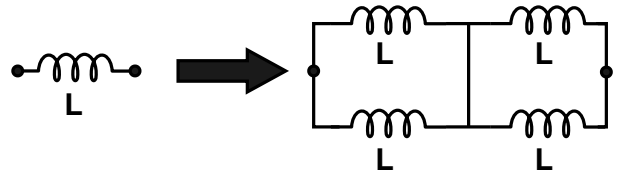


Fig. 4. Setup for investigating contribution to 2nd harmonic generation from inductors. Each inductor was replaced by a constellation of 4 identical inductors. This results in the same inductance value, while both the voltage and current in each inductor decrease to one half of the value for the original single inductor.

signals were averaged over 8 consecutive pulses to reduce noise.

Investigation of nonlinearities in the transmit chain of the ultrasound scanner was the target of this study. Ultrasound pulses measured using a hydrophone will contain both harmonics created in the transmit chain, i.e. present at the transducer surface, and harmonics generated from nonlinear propagation through the water. To reliably access the nonlinearity in the transmit chain, the setup was designed to minimize nonlinear distortion from propagation in water. This was done by placing the hydrophone as close as possible to the probe surface, at 4 mm. In addition, transmitting with only one array element created a diverging wave in the azimuth plane, keeping the acoustic pressure amplitude below 0.6 MPa even at the maximum driving voltage. The actual voltage over the transducer stack was measured using the Pico oscilloscope with an x10 probe (TA386, Pico Technology).

B. Search for sources of 2nd harmonic distortion

Nonlinear distortion in the signal picked up by hydrophone can come from any of the following sources:

- 1) Inductors in the tuning network
- 2) Propagation of the ultrasound pulse in water
- 3) Acoustic stack
- 4) Hydrophone and data acquisition system
- 5) Transmit electronics

Experiments were set up to isolate the effect of these sources, with the aim to identify the main source of the 2nd harmonic observed in the acoustic pulses.

1) *Tuning inductors*: Inductors with core material other than air can behave nonlinearly at high currents, due to saturation of the magnetic flux density in the inductor core. Wölfe and Hurley, using a variable inductance characteristic that is independent of current direction, showed that saturation in the inductor produces only odd harmonics due to the symmetry [19]. However, at very high currents, asymmetric saturation may occur, creating even harmonics as well.

The contribution to 2nd harmonic generation from nonlinearities in the inductors was tested by replacing each of the tuning inductors in Fig. 1 with four inductors of identical type, connected as shown in Fig. 4. This gives the same inductance, but reduces the current through and the voltage over each inductor by a factor 2. Nonlinear distortion in inductors depends on the current and voltage level, hence, if the 2nd harmonics observed in the transmitted pulses are

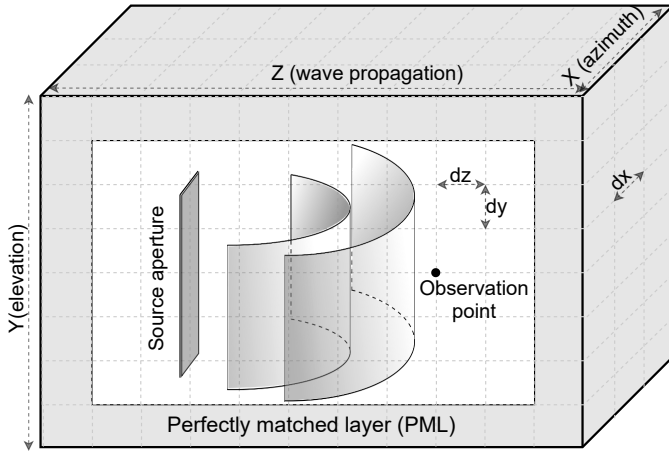


Fig. 5. Schematic illustration of the k-wave simulation model of pulse propagation from the transducer through 4 mm of water to the hydrophone. The source is a rectangular piston matching the element dimension, i.e. long in elevation and narrow in azimuth. The simulation region is enclosed in a perfectly matched layer to simulate infinite space. In the simulations, the pressure at the transducer surface is defined so that its spectrum contains no 2nd harmonic, with an amplitude giving a positive pressure peak of 0.5 MPa at distance 4 mm, i.e. equal to the maximum pressure level found in the measurement, Fig. 9

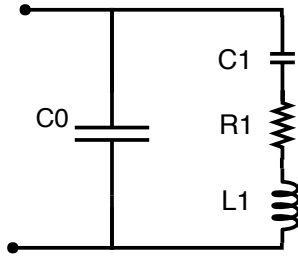


Fig. 6. Passive load used to replace the transducer, creating a Butterworth-Van Dyke circuit with similar impedance characteristics around resonance. The component values are $C0=120$ pF, $C1=50$ pF, $R1=470$ Ω , and $L1=60$ μ H.

caused by the inductors, the level should be reduced by this arrangement.

2) *Simulation of propagation in water:* Ultrasound pulse propagation through water is nonlinear, this is actually the basis for doing harmonic imaging. However, the purpose of this study was to investigate possible nonlinearities in the transmit chain, not in water. Hence, nonlinearities from sound propagation through water would come in as an artifact, and had to be minimized.

Accurate measurements of 2nd harmonic generation from pulse propagation would require an acoustic source known to be linear, even at high pressure level. In the present study, this would mean a source generating the pressure 0.5 MPa with 2nd harmonic level lower than the base noise level, i.e. approximately -45 dB relative to the fundamental frequency. Such a source is difficult to obtain. Instead, the generation of 2nd harmonics by nonlinear propagation was simulated by a nonlinear ultrasound model in *k-Wave* [20], a free, open source Matlab toolbox using the *k*-space pseudo spectral method [21]. The accuracy of *k-wave* for estimating 2nd harmonics

through nonlinear propagation in water has been investigated in [22], showing a good agreement between the simulation and experimental results.

The *k-wave* simulation model is illustrated schematically in Fig. 5. The computational grid for the simulation was selected to cover the transducer aperture and the near field region, set to 3.2 mm \times 12.8 mm \times 6.4 mm ($x \times y \times z$), with grid point spacing 25 μ m. A 5-cycle sine-wave enclosed in a Gaussian envelope was used as the input pressure at the source ($z=0$), i.e. the transducer surface. The observation point is at the hydrophone tip, 4 mm from the center of the source. Note that the source considered here is shaped as one element in the linear array transducer, giving an acoustic field close to a cylindrical wave. A perfectly matched layer (PML) with thickness 0.5 mm was added to simulate the infinite propagation space. The elevation focusing effect of the acoustic lens attached on the transducer surface was simulated by using the curved transducer definition in *k-wave*. Typical values of acoustic parameters for water at 25 $^{\circ}$ C were taken from the literature [23], [24], in some cases by interpolating from measurements at different temperatures. The values are listed in Table I. The parameters used in the *k-wave* simulation are speed of sound c_0 , density ρ , acoustic nonlinearity parameter B/A [25] and attenuation α_0 . The pressure amplitude at the source was selected so that the simulated pressure at 4 mm had the same value as the measured pressure at this position, 0.5 MPa.

TABLE I
ACOUSTIC PARAMETERS FOR WATER, USED IN THE *k*-WAVE SIMULATION.

c_0	ρ	B/A	α_0
m/s	kg/m ³		dB/(MHz ² cm)
1496	997	5.2	0.0019

3) *Acoustic stack:* Nonlinearity in the acoustic part of the system was checked by replacing the acoustic stack with a passive electric load having a similar electrical impedance. This gives similar electrical loading, i.e. current and voltage, as the active transducer element. If the same 2nd harmonic level is seen in the voltage V_s measured over this dummy load, see Fig. 1, it must come from nonlinearities in the electric transmit chain, i.e. generator, amplifier, tuning and cable assembly. On the other hand, if the 2nd harmonic in V_s vanishes after replacing the acoustic stack with the passive load, transmit electronics cannot be the source, and this 2nd harmonic must then come from the acoustic stack. A passive load can never perfectly reproduce the impedance of the piezoelectric stack, but a close approximation can be achieved with a Butterworth-Van Dyke (BVD) network [26], [27], illustrated in Fig. 6. Values for the electric components were selected to match the impedance of the acoustic stack around its resonance frequency, as listed in Fig. 6.

4) *Hydrophone and data acquisition system:* A hydrophone should be linear, but no quantitative information of linearity was provided for the hydrophone used in this study. Hydrophone nonlinearity, if present, might occur for very high acoustic pressures, and investigation of this should be done at the highest acoustic pressure used in this study. Hydrophone nonlinearity was tested by transmitting ultrasound pulses giv-

ing at least 0.5 MPa at the hydrophone tip, and recording and analysing these pulses. The 2nd harmonic level measured by this method will give an upper bound to potential 2nd harmonics generated in the hydrophone and receiver chain.

The test was done by comparing two pulses giving similar pressure amplitudes at the hydrophone tip: 1) Pulses generated by one transducer element driven at 80 V voltage amplitude, and 2) pulses generated from 16 transducer elements, focused to the hydrophone tip and driven to give the same pressure amplitude as with one element. To be able to drive and focus the 16 elements, the transmit stage of the clinical scanner was used. Hence, this experiment was done with 5-cycle long square-wave excitation pulses, not the Gaussian-shaped pulses used in the other experiments. The measurement setup was as in Fig. 1, with the signal generator and power amplifier replaced the transmit electronics of a clinical scanner, and 16 elements were excited to get a beam focused at the hydrophone tip. The excitation voltage required to reach the same pressure amplitude when using 16 elements and focusing was found to be 10 V.

5) *Excitation sources*: In this part, two different excitation sources used in this paper are investigated for their 2nd harmonic distortion. The first one, used in most measurements, was the external excitation source, comprising a function generator and a power amplifier. 2nd harmonic distortion from this source was investigated by measuring its output into a 50 Ω terminator at the highest voltage level used in the study.

The second excitation source was the clinical scanner, creating square-wave excitation. This is made so that it can only transmit when the probe is connected, making it difficult to measure the 2nd harmonic without including the effect of the probe. To overcome this limitation, an alternative method to test its nonlinearity was found. The excitation waveforms were measured when driving one element in the array transducer, and compared to when driving two elements connected in parallel Fig. 7. In the latter case, the current from the pulser will be twice of that in the first case, and nonlinearities from the pulser should change, altering the 2nd harmonic level. If the driving waveforms are identical when driving one element compared to when driving two elements in parallel, the pulser can be assumed to be linear.

C. Nonlinear impedance of the acoustic stack

Besides 2nd harmonic generation, another manifestation of nonlinearity in the acoustic stack would be a voltage dependency in the impedance. When excited at a single angular frequency ω_0 , a nonlinear impedance can lead to harmonic terms in both voltage and current, so that the total current I through and voltage V over the acoustic stack will contain both the driving frequency ω_0 and its harmonics,

$$V = \sum_{n=0}^{\infty} \hat{V}_n e^{j(n\omega_0 t)} \quad I = \sum_{n=0}^{\infty} \hat{I}_n e^{j(n\omega_0 t)}, \quad (1)$$

where n is an integer number representing the harmonics, and \hat{V}_n, \hat{I}_n are complex numbers giving the amplitude and phase of the harmonic terms in the voltage and current. The frequency dependent impedance $Z(\omega)$ is defined for a linear system. In

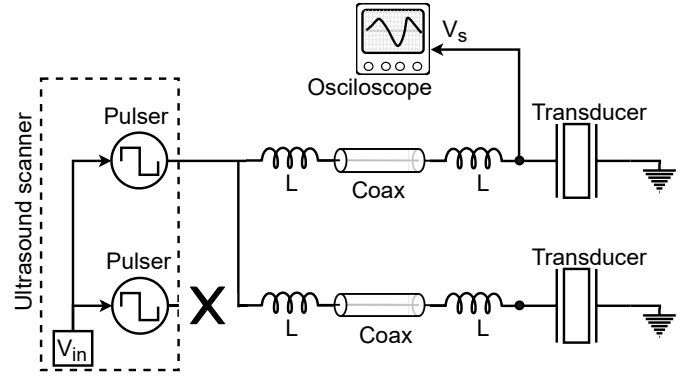


Fig. 7. Experimental setup for testing 2nd harmonic generation in the 3-level pulser mode inside the clinical ultrasound scanner. One element channel was disconnected from its pulser, and connected in parallel with another channel. The amplitude of the pulser's output voltage, V_{in} , was programmed in the ultrasound scanner, and the voltage over the transducer stack, V_s , was measured.

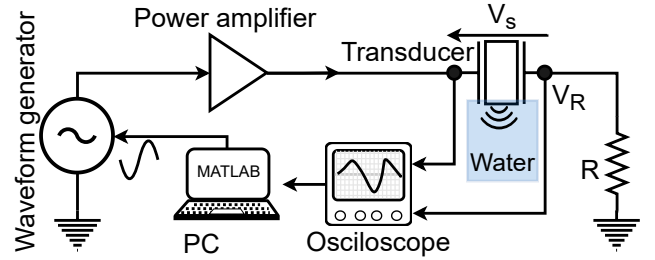


Fig. 8. Experimental setup for measuring the electrical impedance at different voltage levels. Narrow band sine-wave bursts are swept through a range of frequencies and voltage amplitudes. The voltage and current over the transducer are measured. The resulting impedance curve is obtained by finding the ratio of voltage to current at each frequency f_0 within the sweep.

presence of nonlinearities, the definition is not straightforward. In this study, we have chosen to look at the ratio of voltage $V(\omega)$ to current $I(\omega)$ at the fundamental frequency ω_0 only, and define the fundamental electrical impedance $Z_1(\omega_0)$ at the driving angular frequency ω_0 as

$$Z_1(\omega_0) = \hat{V}_1(\omega_0) / \hat{I}_1(\omega_0). \quad (2)$$

Following this definition, the impedance curve $Z_1(\omega_0)$ for the acoustic stack was investigated at different applied voltage levels $V(\omega_0)$, using the measurement setup in Fig. 8. The waveform generator output was amplified by the power amplifier. The amplifier was connected directly to the acoustic stack, without any electric matching network. The current through the stack was found by adding a 10 Ω resistor in series and measuring the voltage V_R over this resistor.

The power amplifier was designed to work with a 50 Ω load, and its output voltage is influenced by the load impedance. The acoustic stack's impedance varies with frequency, in particular around the resonant and anti-resonant frequencies, causing the output voltage from the amplifier to change with frequency for a given input voltage. To ensure the impedance was investigated under constant voltage, the voltage over the stack was recorded by the oscilloscope, and used as feedback to the generator. This was used to scale the generator output,

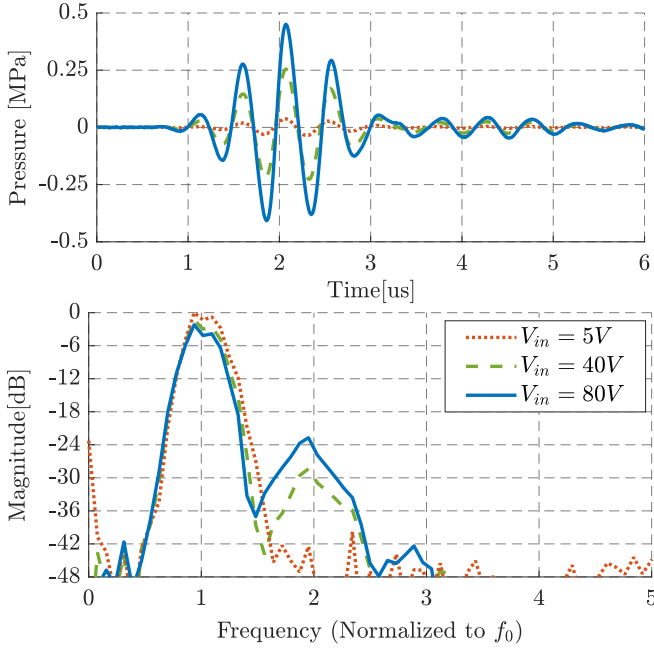


Fig. 9. Acoustic pressure measured 4 mm from the transducer surface, for different excitation voltages. Distinct peaks are seen at the 2nd harmonic frequency for the two highest driving voltages. The spectra were normalized to the input voltage amplitude.

maintaining a constant voltage amplitude over the stack when sweeping over the frequency range.

The excitation signals were the same 5-cycle Gaussian enveloped sine-waves as the previous setup, sweeping the center frequencies ω_0 over the range to be studied. Voltage $v(t)$ and current $i(t)$ over the acoustic stack were measured as function of time t , and transformed into the frequency domain using fast Fourier transform (FFT) without windowing. Since the excitation signals are tapered pulses, taking FFT without further windowing does not cause significant spectral leakage. At each frequency step, the impedance was calculated by dividing the voltage $V(\omega_0)$ by the current $I(\omega_0)$ at the center frequency f_0 of the pulse. The measurements were done as upward frequency sweeps from 1 MHz to 6 MHz in steps of 0.1 MHz. At each frequency step, the voltage amplitude was increased from 20 V to 120 V. From these measurements, the impedance of the stack at different driving voltage amplitudes were calculated. The measurement procedure was repeated after replacing the acoustic stack with the passive load shown in Fig. 6. The impedance curves of the stack and of the passive load were also measured using a vector network analyzer (R&S ZVL, Rohde & Schwarz, Germany), for comparison with a standard reference instrument.

D. Temperature effects

All measurements were done at room temperature using 5-cycle pulses. These short pulses were selected to avoid a temperature increase in the transducer element during the measurements. The pulse repetition frequency was 100 Hz, corresponding to a duty-cycle of 1/2000 for the longest pulse

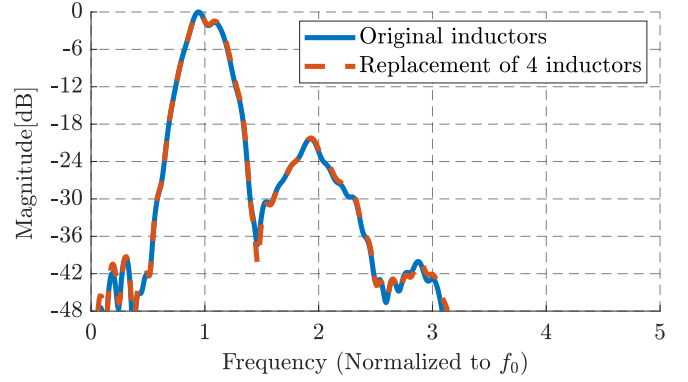


Fig. 10. Acoustic pressure measured 4 mm from the transducer surface, with the original tuning inductors (blue, solid), and with each inductor replaced by the group of 4 inductors shown in Fig. 4 (red, dashed). No difference can be seen between the two measurements.

at 1 MHz, which gives the transducer time to return to the ambient temperature between each pulse. A very low pulse repetition frequency, 1 Hz, was also tested at the highest voltage. Results at this pulse repetition frequency could not be distinguished from the results obtained at 100 Hz, confirming that the results were not influenced by element self-heating. The transducer surface was in water during the measurements, ensuring good heat dissipation from the transducer. Based on this, temperature effects during the measurements were considered negligible.

III. RESULTS

A. Second harmonic in the transmitted pulses

The transmitted ultrasound pulses, measured by the hydrophone setup in Fig. 1, are shown in Fig. 9. The input voltage amplitudes are 5 V, 40 V, and 80 V and the 5-cycle Gaussian sine-wave excitation was used. The spectra in Fig. 9 show a distinct peak at the 2nd harmonic frequency for the two highest driving voltages. For the highest voltage, 80 V, this peak is 20 dB below the peak at the transmit frequency. A similar 2nd harmonic level was found when driving the transducer with a 5-cycle square-wave excitation from the clinical scanner, see Fig. 13. In this configuration, the spectrum of the pulse from one element driven with 80 V gives a distinct peak of -19 dB at the 2nd harmonic.

B. Dependence on transmit chain

1) *Tuning inductors*: Replacing each inductor in the tuning circuit by the group of 4 inductors shown in Fig. 4 caused no measurable difference in the received pulses for any driving voltage, see Fig. 10. This rules out the inductors as a source of the observed 2nd harmonic.

2) *Nonlinear propagation in water*: Results of the k-wave simulations done to check for nonlinear propagation in water are presented in Fig. 11. After 4 mm propagation distance through water, the simulations predict a 2nd harmonic level at -35 dB relative to the fundamental frequency. This is 11 dB below the -24 dB observed in the measured ultrasound pulse

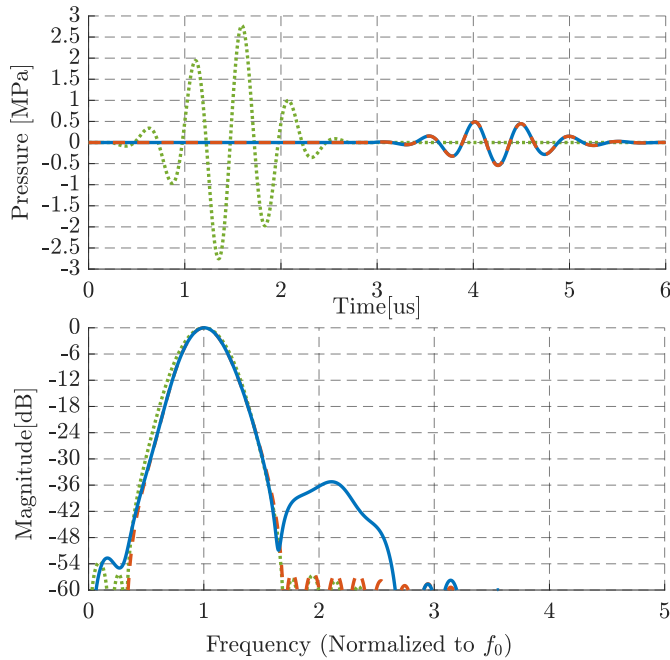


Fig. 11. K-wave simulation of pulse propagation through water. Pulse shapes at the transducer surface (green, dotted) and after 4 mm propagation distance including (blue, solid) and neglecting (red, dashed) water nonlinearity. This result predicts a 2nd harmonic level from nonlinear propagation to 35 dB below the level at the fundamental frequency for pulse pressure amplitude 0.5 MPa.

in Fig. 9. Sensitivity to position was checked by repeating the simulations with the receiver moved within a region ± 1 mm from the original position, both laterally and axially. The observed variation in 2nd harmonic level within this range was within ± 1 dB.

3) *Acoustic stack*: Voltages V_s measured over the acoustic stack are shown in Fig. 12, compared with the voltages after replacing the stack with a passive load described in Fig. 6. With the acoustic stack (unmarked bold lines), a 2nd harmonic peak at -25 dB was seen for the highest voltage, $V_{in}=80$ V, while none was seen for $V_{in}=5$ V. When the acoustic stack was replaced by the passive load of similar impedance (marked thin lines), no peak at the 2nd harmonic could be seen, for any driving voltage. The noise floor is 45 dB below the level at the fundamental frequency. The experiment was repeated using the 3-level pulser mode in the clinical scanner to drive the transducer, giving the same result. These results demonstrate that the 2nd harmonic observed with the transducer connected cannot originate from nonlinearities in the electrical transmit circuitry, comprising the excitation sources, cable, and tuning network.

4) *Hydrophone and data acquisition system*: The next test investigated possible contributions to nonlinear distortion from the data acquisition system, including the hydrophone, its dedicated amplifier, and the recording oscilloscope. The result is shown in Fig. 13. The reference pulse with pressure amplitude 0.6 MPa was created using 16 transducer elements, excited at voltage amplitude $V_{in}=10$ V. The 2nd harmonic level from this pulse is -33 dB relative to the maximum. Note

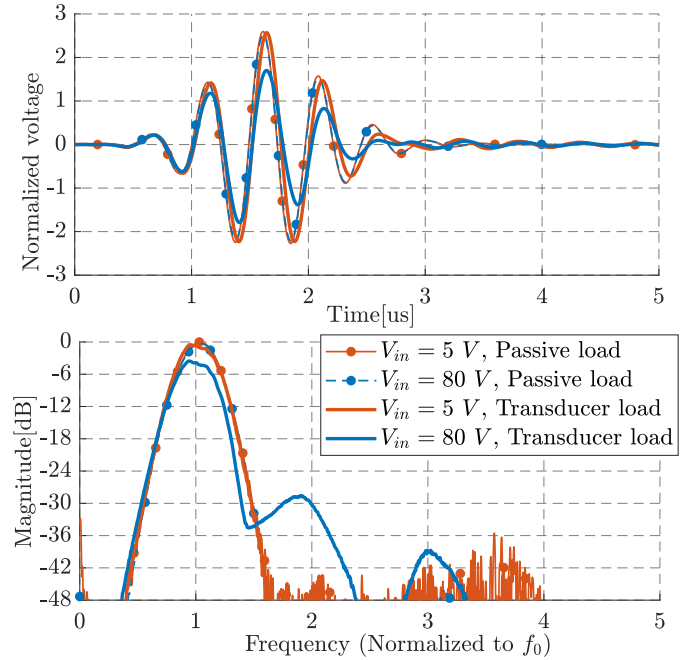


Fig. 12. Voltage measured over the acoustic stack, before and after replacing the stack with a passive load of similar impedance, Fig. 6. No 2nd harmonic peak can be seen when using the passive load (marked thin lines), for any voltage. For the transducer load (unmarked bold lines), peaks are seen at the 2nd and 3rd harmonics at the highest voltage, 80 V. The results were normalized to the input voltage amplitude V_{in} .

that the clinical scanner was used to drive the transducer, as the arbitrary waveform source could not drive 16 elements and focus the beam. This result puts an upper bound to 2nd harmonics created by the acquisition system at pressure amplitude 0.6 MPa to -33 dB. For comparison, a similar pulse was generated by a single transducer element, driven by the same 3-level waveform but at voltage amplitude $V_{in}=80$ V. From Fig. 13 it is seen that this pulse has the same pressure level, shape and spectrum as the reference pulse from 16 elements, except for the level at the harmonics. The 2nd harmonic level in this pulse is -19 dB, indicating that the main source for 2nd harmonic distortion is not the acquisition system.

5) *Excitation sources*: The signal generator with the power amplifier connected to a 50Ω terminator and driven at the highest voltage, 80 V. In this configuration, the 2nd harmonic level was below -50 dB relative to the fundamental. This is at the noise level of the power amplifier and around 25 dB below the 2nd harmonic level observed with the transducer connected, Fig. 12.

The 3-level pulser was tested by measuring the voltage over the stack with two element channels connected in parallel, and comparing this result to the voltage with one channel connected. Driving two channels in parallel will approximately double the pulser output current, and should increase 2nd harmonics originating in the pulser. The increased loading from two channels caused the voltage V_s to drop, and reduced the 2nd harmonic originating in the channels. For a straight-forward comparison, the nominal voltage V_{in} , i.e. the voltage

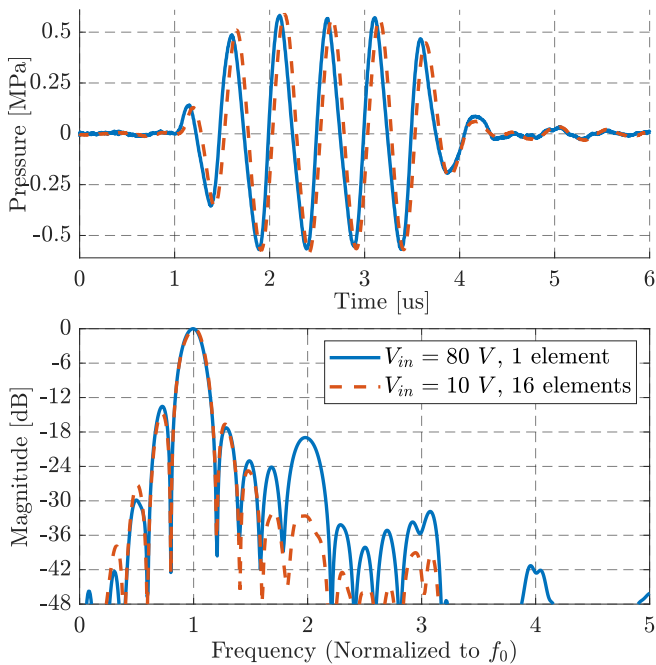


Fig. 13. Pressure measured by the hydrophone when exciting 1 element (blue, solid) or 16 elements (red, dashed) in the probe. The driving voltage was adjusted to give identical output pressures.

amplitude programmed into the scanner, was reduced from 80 V to 63 V to give the same voltage V_s measured across the stack when one channel was connected. The results in Fig. 14 show that the 2nd harmonic levels are equal when the voltages measured over the stack are equal, i.e. when $V_{in}=63$ V for one element and $V_{in}=80$ V for two elements in parallel. In the latter case, the current from the pulser doubles, but the 2nd harmonic level is unchanged. This indicates that the 2nd harmonic level depends on the voltage amplitude over the acoustic stack but does not originate from the pulser.

C. Nonlinear impedance of the acoustic stack

The electrical impedance of the transducer was measured by sweeping the center frequency from 1 to 6 MHz at 0.1 MHz intervals, using the setup in Fig. 8. Nonlinearity was tested by using three different voltage amplitudes, $V_{s,max}=20$ V, 60 V, and 120 V. The results are plotted in Fig. 15. As the excitation voltage increases, the impedance magnitude decreases and the impedance phase increases. The results were checked by comparing with measurements done by a network analyzer using low voltage. The network analyzer results were found to agree very well with the impedances measured at the lowest driving voltage amplitude, $V_{s,max}=20$ V.

This procedure was repeated to measure the impedance in the passive load in Fig. 6. The results are plotted in Fig. 16, showing no difference between the three measured impedance curves, i.e. frequency sweeping at low and high voltages, and the result from the network analyzer. This confirms that the impedance of the passive load is linear, that its impedance is very similar to that of the acoustic stack, and it validates

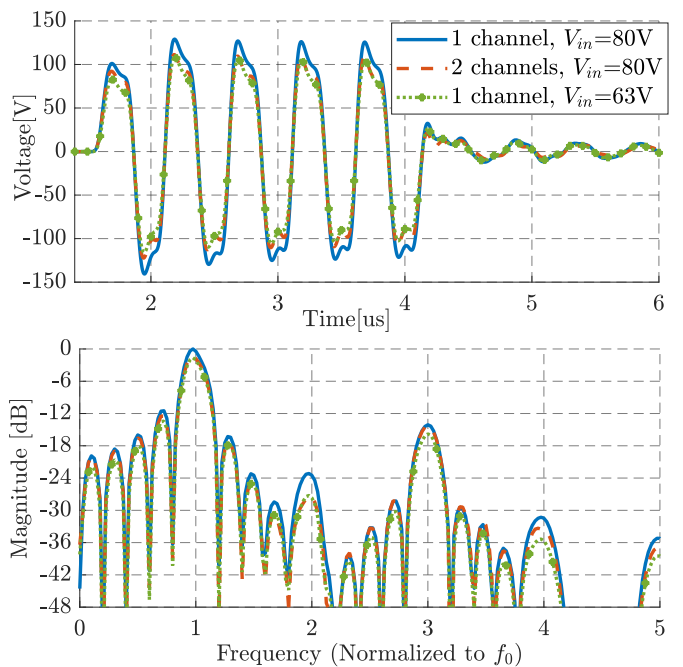


Fig. 14. Voltage V_s measured over the acoustic stack, driven by the clinical scanner at the highest level $V_{in}=80$ V, with one element connected (blue, solid) and two elements in parallel (red, dashed). Connecting two elements reduced the voltage over the stack, decreasing the 2nd harmonic level by approximately 3 dB. The results for two elements in parallel at $V_{in}=80$ V were identical to results when driving one element with $V_{in}=63$ V (green, dotted), at both the fundamental and 2nd harmonic frequencies.

the impedance measurement setup for high voltages shown in Fig. 8.

IV. DISCUSSION

A. Second harmonic generation

Summary of the second harmonic levels in different measurements were listed in Table II. If assuming a worst-case scenario, at the highest voltage, $V_{in}=80$ V, the maximum 2nd harmonic levels from the electrical circuit, -45 dB, water propagation, -35 dB, and the hydrophone, -33 dB, can add up to -27 dB, if all contributions are in phase. A more realistic scenario is incoherent summing, giving -31 dB. The measured 2nd harmonic level in the transmitted pulse is -20 dB. This cannot be explained by any combined effect of the three sources above, and it is concluded that the main source of 2nd harmonic in the pulse must be caused by nonlinear effects in the transducer stack.

The hydrophone was positioned on the acoustic axis 4 mm from the front face of the transducer. The acoustic axis was found by the Onda AIMS II measurement system by scanning the beam profile and selecting the center position. The positioning stage have resolution of 0.1 mm, and correctly estimating the center position comes with some uncertainty. However, the k-wave simulations predict less than 1 dB variation in 2nd harmonic level when the hydrophone is moved over a range ± 1 mm from the estimated position, and uncertainty caused by hydrophone position is considered negligible.

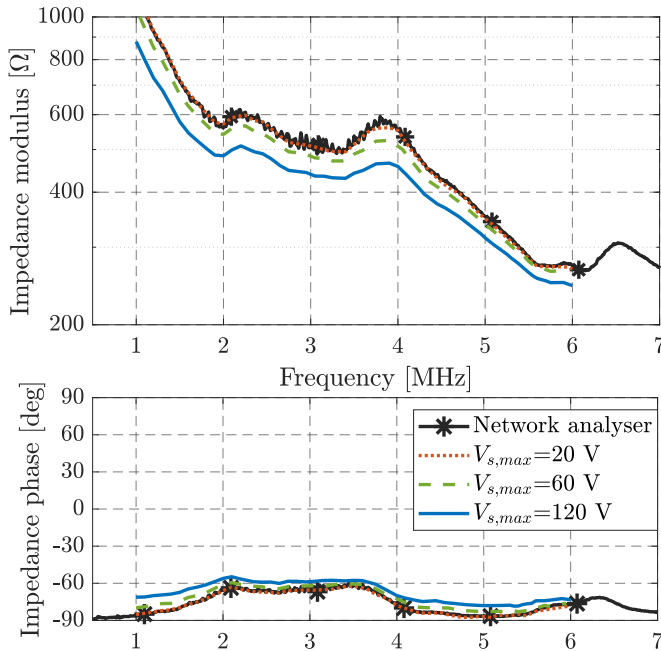


Fig. 15. Impedance curve of the acoustic stack measured by sweeping the center frequency of the excitation voltage, at voltage amplitudes 20 V, 60 V, and 120 V. After the test, the impedance curve was measured again using a network analyzer to confirm that the acoustic stack was not depoled under high excitation voltage during the test.

The maximum electric field in the active layer, a single crystal PMN-PT, was 5.8 kV/cm. A strong electric field may depole and damage the transducer if higher than the coercive field of the material used in the stack and applied for a long time. The coercive field in single crystal PMN-PT is not well characterized at the frequency ranges used in medical ultrasound. Wei-Gen et al. [28] reported a coercive field of 3.5 kV/cm for $\langle 001 \rangle$ oriented 0.67PMN-0.33PT, using 2 ms duration triangular pulses, i.e. around 1000 times longer than what was used in this study. On the other extreme, Zhang and Li [29] studied much shorter pulses, with duration 10 ns and duty cycle smaller than 1%. They found that under these conditions the pulse amplitude could be three times the coercive field without any depoling occurring. Depoling will permanently change the electrical impedance of the transducer. In this study, the transducer impedance was measured before and after the experiments, and the results were identical. This verifies that no permanent depoling occurred.

The impedance of the passive RLC-circuit used to replace the transducer is similar but not perfectly identical to the transducer impedance. The circuit was designed so that the impedance magnitude of the passive load is smaller than the transducer impedance for all frequencies. A lower impedance magnitude causes a higher current in the circuit, which should enhance nonlinearities. Despite this, no 2nd harmonic generation was observed when using the passive load.

Parentoine et al. [16] reported that in the piezoelectric material, the mechanical nonlinearity dominates the piezoelectric mechanism while the influence of electrical nonlinearity was

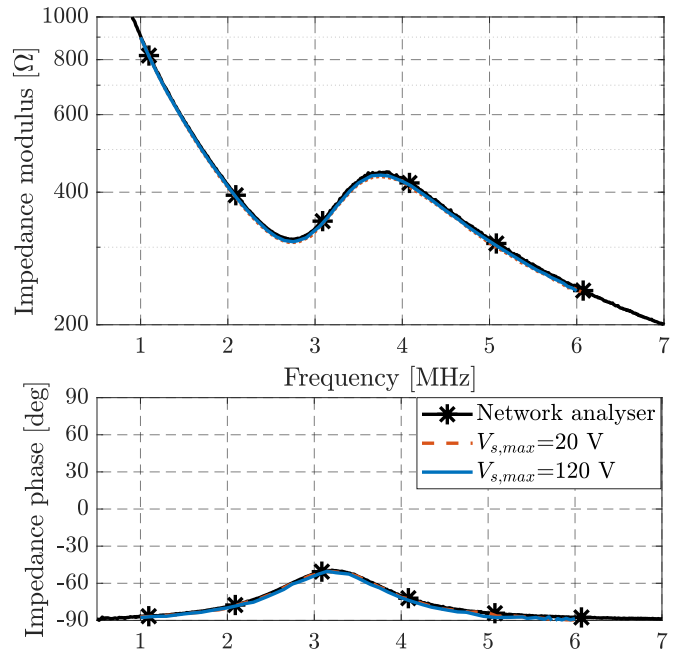


Fig. 16. Impedance of the passive load, Fig. 6, measured at high voltages using the setup in Fig. 8 and using the network analyzer. The three resulting curves cannot be distinguished. This verifies that the passive load is linear with impedance very similar to that of the acoustic stack.

very small and could be neglected [30]. Perez and Albareda [11] also used the same assumption. Note however that the experimental situation used in these studies was different from that in our study. Perez and Albareda excited piezoelectric samples of simple geometry in free vibration conditions, where a low electric field can create very high mechanic strain. In our study, the piezoelectric element is mechanically loaded by an acoustic lens and a water column, causing a higher mechanical load. Under these conditions, a stronger electric field is needed to create the same strain. Hence, the result from [11] may not be directly transferable, and nonlinearity in both dielectric, piezoelectric and mechanical coefficients should be considered. Our study cannot distinguish between effects from different mechanisms in the piezoelectric material. In addition, nonlinear effects in the other layers in the acoustic stack, i.e. backing, matching and bonding layers, may also be sources for the observed nonlinear effects.

We have listed and investigated possible sources for nonlinearity nonlinear in a clinical ultrasound scanner. The results identified the acoustic stack as the main source for nonlinear distortion in pulses transmitted from the transducer. The result is strictly valid only for the scanner and probe investigated in this study. But the measurement procedure can be applied to other ultrasound systems, with different transmit electronics and other types of ultrasound transducers, to identify and quantify sources for nonlinearity in these systems.

B. Nonlinear impedance of the acoustic stack

Fig. 15 shows how the impedance changes with the voltage amplitude $V_{s,max}$ over the stack. By plotting the stack admit-

TABLE II
SECOND HARMONIC LEVELS IN DIFFERENT MEASUREMENT CONFIGURATIONS.

Experiment	Included components (indicated in Fig. 1)					Result 2nd harmonic level (dB)
	5 Transmit electronics	1 Electric tuning circuitry	3 Acoustic stack	2 Water propagation path	4 Hydrophone with acquisition system	
Whole chain	✓	✓	✓	✓	✓	-18
Inductors	✓	Replaced by 4 inductors	✓	✓	✓	-18
Waveform generator and amplifier driving 50Ω terminator	✓	-	-	-	-	-50
K-wave simulation	-	-	-	✓	-	-35
Piezoelectric stack replaced by RLC-circuit	✓	✓	-	-	-	-45
Focused beam using 16 elements driven at low voltage	Replaced by 16 parallel channels at low voltage			✓	✓	-33

tance $Y = G + iB$ in the conductance-susceptance plane, as a $G - B$ plot, it can be seen that the curves shift towards higher conductance and higher susceptance when increasing the voltage. This shift can be modeled by separating the admittance curve $Y(f)$ measured at different voltage amplitudes into two parts as

$$Y(f, V_{s,max}) = Y_0(f) + \Delta Y_{NL}(f, V_{s,max}) \quad (3)$$

where $Y_0(f) = G_0 + iB_0$ is the admittance curve at low voltage, and ΔY_{NL} the nonlinear admittance variation. Fig. 17 shows that the admittance curve shifts in the same direction for all frequencies, and increases approximately linearly with the voltage amplitude. This suggests that the nonlinear part can be adequately modeled by assuming it only depends on the voltage amplitude over the stack $V_{s,max}$,

$$\Delta Y_{NL}(f, V_{s,max}) = \Delta Y_{NL}(V_{s,max}), \forall f, \quad (4)$$

and that this dependence is a linear function of $V_{s,max}$ that can be written as

$$\Delta Y_{NL}(V_{s,max}) = (g + ib)V_{s,max}, \quad (5)$$

or

$$Y(f, V_{s,max}) = G + iB = G_0 + gV_{s,max} + i(B_0 + bV_{s,max}) \quad (6)$$

The coefficients g and b define the direction and magnitude of the admittance shift, i.e. how much the conductance G and susceptance B change per unit voltage increase in $V_{s,max}$. This expression is similar to Albareda's approach [14] but formulated in terms of conductance and susceptance. Albareda modeled the deviation in impedance ΔZ around resonance as proportional to the square of the current. Another approach was used by Gonnard [13] who introduced two non-linear elements in series at the input of the electro-mechanical equivalent circuit, proportional to the current density and inversely proportional to the square of the frequency.

The values of g and b were calculated using curve fitting to minimize the mean squared difference between the estimated admittance curve given by (3) and the measurement at different voltage levels. These resulting values were $g = 0.004 \text{ mS/V}$ and $b = 0.0018 \text{ mS/V}$.

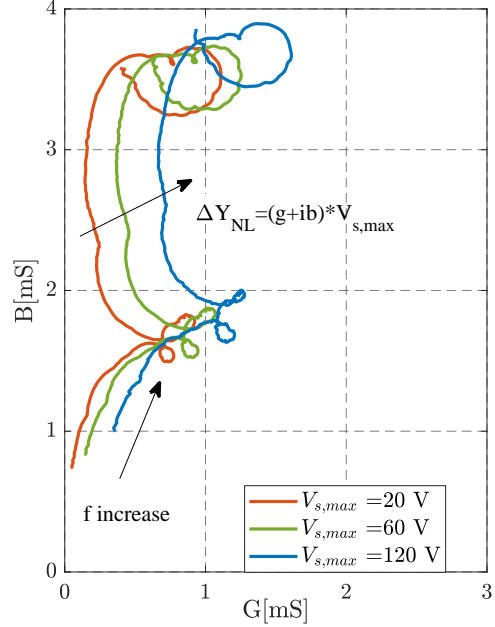


Fig. 17. Admittance of the acoustic stack in the G - B plane for different excitation voltages and frequencies. The admittance can be modeled as the sum of a constant admittance term and a nonlinear component proportional to the voltage amplitude.

C. Voltage and current over the stack

The measurements using the setup in Fig. 8 gave voltage and current over the stack for different driving voltages. These are plotted in Fig. 18 for the highest stack voltage, $V_{s,max}=120 \text{ V}$. Note that in this setup, the acoustic stack was connected directly into the power amplifier output. The 2nd harmonic level in the measured *voltage* curve is very low, around the noise level -45 dB . However, the 2nd harmonic in the measured *current* is much higher, -25 dB . A linear stack impedance cannot explain this, linear behavior predicts the same level of 2nd harmonic for current and voltage. Hence, the high 2nd harmonic in current but not in voltage indicates a nonlinear impedance in the acoustic stack. This is in agreement with the previous conclusion that the stack is the main source of the observed 2nd harmonic in the ultrasound pulses.

The relative 2nd harmonic level of voltage and current as function of measured voltage amplitude $V_{s,max}$ are plotted in

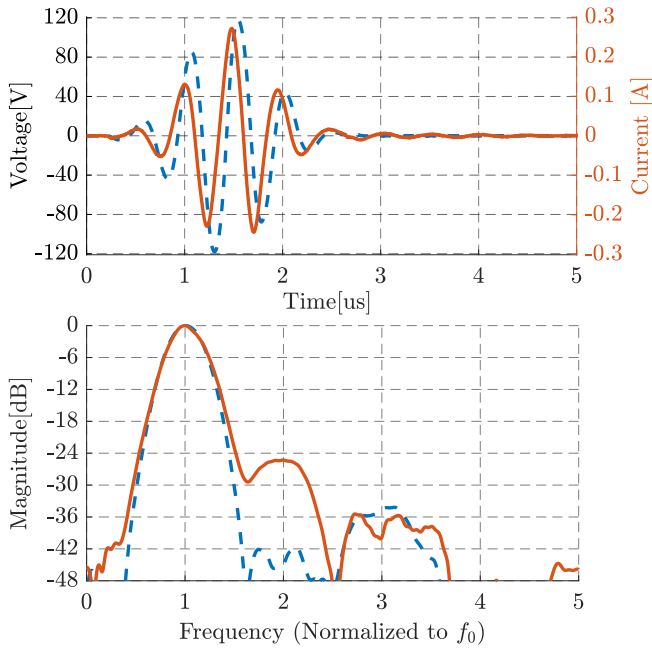


Fig. 18. Voltage (dashed, blue) and current (solid, red) over the stack at the highest voltage level at frequency 2 MHz. The 2nd harmonic levels are -25 dB in current and -45 dB in voltage.

Fig. 19. This result shows an increase of the 2nd harmonic level, relative to the fundamental, for both voltage and current as the voltage amplitude increases. Note that the 2nd harmonic level in the voltage is very low, close to the noise limit, and it cannot be stated whether this is due to the transducer, the amplifier, or some noise source. The 2nd harmonic level in the current measurement is much higher and is a clear manifestation of stack nonlinearity.

Note also that with the setup in Fig. 1, where the tuning board is included, the acoustic stack 2nd harmonic voltage, plotted in Fig. 12, is high, -25 dB at driving voltage $V_{in}=80$ V. This corresponds to a voltage $V_{s,max}=120$ V over the acoustic stack. This indicates that the individual 2nd harmonic levels in the voltage and current also depend on the output impedance of the excitation source. Hence, it is not possible to separate between nonlinear effects caused by the current and caused by the voltage.

V. CONCLUSION

This study has investigated sources of nonlinear distortion in ultrasound pulses transmitted from a clinical ultrasound probe. At distance 4 mm from the probe, we measured 2nd harmonic levels up to -20 dB relative to the fundamental frequency, at pressure amplitude 0.5 MPa.

Investigation of the possible sources for this nonlinearity eliminated transmitter electronics, tuning inductors, propagation through the water and the data acquisition system, leaving the electro-acoustic transducer stack as the main source of the nonlinearity. When the acoustic stack was replaced by a passive load of similar impedance, no 2nd harmonic was seen. We conclude that nonlinearity in the acoustic stack is

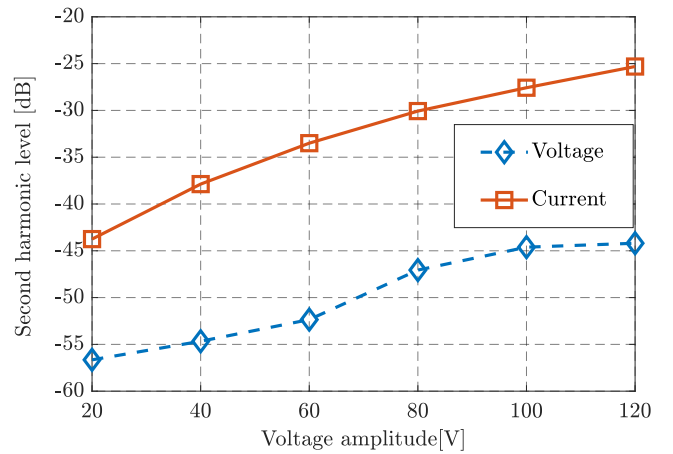


Fig. 19. 2nd harmonic level in current and voltage as function of the voltage amplitude over the stack, measured at frequency 2 MHz

the dominating source of the observed 2nd harmonic. This source can be modeled by a nonlinear electrical impedance, distorting the driving voltage and current, and may come from nonlinear material coefficients in the acoustic stack.

Current and voltage measurements at different excitation voltages showed that the impedance magnitude in the transducer stack shifted downwards over the whole investigated frequency range, from 1 to 6 MHz, as the voltage amplitude increased.

The highest driving voltages tested in this study were above what is used during conventional operation of the probe. These were selected to investigate the phenomenon and push the system to the limit.

ACKNOWLEDGMENT

This work was supported by the Research Council of Norway, project number 237887.

REFERENCES

- [1] M. Averkiou, "Tissue harmonic imaging," in *2000 IEEE Ultrasonics Symposium. Proceedings. An International Symposium (Cat. No.00CH37121)*, vol. 2, pp. 1563–1572, IEEE, 2000.
- [2] F. Tranquart, N. Grenier, V. Eder, and L. Pourcelot, "Clinical use of ultrasound tissue harmonic imaging," *Ultrasound in Medicine & Biology*, vol. 25, pp. 889–894, 7 1999.
- [3] T. S. Desser and R. Jeffrey, "Tissue harmonic imaging techniques: Physical principles and clinical applications," *Seminars in Ultrasound, CT and MRI*, vol. 22, pp. 1–10, 2 2001.
- [4] B. Ward, A. C. Baker, and V. F. Humphrey, "Nonlinear propagation applied to the improvement of resolution in diagnostic medical ultrasound," *J Acoust Soc Am.*, vol. 101, pp. 143–154, 1 1997.
- [5] K. Spencer, J. Bednarz, P. Rafter, C. Korcarz, and R. Lang, "Use of harmonic imaging without echocardiographic contrast to improve two-dimensional image quality," *The American Journal of Cardiology*, vol. 82, pp. 794–799, 9 1998.
- [6] T. S. Desser, T. Jedrzejewicz, and C. Bradley, "Native tissue harmonic imaging: basic principles and clinical applications," *Ultrasound Quarterly*, vol. 16, no. 1, pp. 40–48, 2000.
- [7] T. Huynh, G. Haugen, and L. Hoff, "Reduction of transmitted 2 nd harmonics using an adaptive method by simulated annealing," in *2017 IEEE International Ultrasonics Symposium (IUS)*, pp. 1–4, IEEE, 9 2017.

- [8] A. Lohfink and P.-C. Eccardt, "Linear and nonlinear equivalent circuit modeling of CMUTs." *IEEE transactions on ultrasonics, ferroelectrics, and frequency control*, vol. 52, pp. 2163–72, 12 2005.
- [9] X. Kang, F. Yang, X. H. A. M. Sinica, and U. 2012, "Nonlinearity analysis of piezoelectric micromachined ultrasonic transducers based on couple stress theory," *Springer*, 2011.
- [10] M. Planat and D. Hauden, "Nonlinear properties of bulk and surface acoustic waves in piezoelectric crystals," *Ferroelectrics*, vol. 42, pp. 117–136, 5 1982.
- [11] R. Perez and A. Albareda, "Analysis of nonlinear effects in a piezoelectric resonator," *J Acoust Soc Am.*, vol. 100, no. May, pp. 3561–3569, 1996.
- [12] G. Sebald, L. Lebrun, and D. Guyomar, "Modeling of elastic nonlinearities in ferroelectric materials including nonlinear losses: application to nonlinear resonance mode of relaxors single crystals," *IEEE Trans Ultrason Ferroelectr Freq Control*, vol. 52, pp. 596–603, 4 2005.
- [13] P. Gonnard, "Investigation on dielectric, mechanical and piezoelectric non-linearities in piezoceramics through a new equivalent circuit," in *ISAF 2000. Proceedings of the 2000 12th IEEE International Symposium on Applications of Ferroelectrics (IEEE Cat. No.00CH37076)*, vol. 2, pp. 691–694, IEEE, 2000.
- [14] A. Albareda, P. Gonnard, V. Perrin, R. Briot, and D. Guyomar, "Characterization of the mechanical nonlinear behavior of piezoelectric ceramics," *IEEE Trans Ultrason Ferroelectr Freq Control*, vol. 47, no. 4, pp. 844–853, 2000.
- [15] R. Ozaki, Y. Liu, H. Hosaka, and T. Morita, "Piezoelectric nonlinear vibration focusing on the second-harmonic vibration mode," *Ultrasonics*, vol. 82, pp. 233–238, 1 2018.
- [16] D. Parenthoine, L. Haumesser, F. Meulen, M. Lethiecq, and L.-P. Tran-Huu-Hue, "Nonlinear constant evaluation in a piezoelectric rod from analysis of second harmonic generation," *IEEE Trans Ultrason Ferroelectr Freq Control*, vol. 56, pp. 167–174, 1 2009.
- [17] W. Wang, S. Wang, Y. Zhang, X. Zhao, and H. Luo, "Beam-Mode Piezoelectric Properties of Ternary $\text{Pb}(\text{In}_{1/2}\text{Nb}_{1/2})\text{O}_3\text{-Pb}(\text{Mg}_{1/3}\text{Nb}_{2/3})\text{O}_3\text{-PbTiO}_3$ Single Crystals for Medical Linear Array Applications," *Journal of Electronic Materials*, vol. 40, pp. 2228–2233, 11 2011.
- [18] R. Zhang, B. Jiang, and W. Cao, "Elastic, piezoelectric, and dielectric properties of multidomain $0.67\text{Pb}(\text{Mg}_{1/3}\text{Nb}_{2/3})\text{O}_3\text{-}0.33\text{PbTiO}_3$ single crystals," *Journal of Applied Physics*, vol. 90, pp. 3471–3475, 10 2001.
- [19] W. Wolffe and W. Hurley, "Quasi-active power factor correction with a variable inductive filter: theory, design and practice," *IEEE Transactions on Power Electronics*, vol. 18, pp. 248–255, 1 2003.
- [20] B. E. Treeby, J. Jaros, A. P. Rendell, and B. T. Cox, "Modeling nonlinear ultrasound propagation in heterogeneous media with power law absorption using a k-space pseudospectral method," *J Acoust Soc Am*, vol. 131, pp. 4324–4336, 6 2012.
- [21] G. F. Pinton and G. E. Trahey, "A comparison of time-domain solutions for the full-wave equation and the parabolic wave equation for a diagnostic ultrasound transducer," *IEEE Transactions on Ultrasonics, Ferroelectrics, and Frequency Control*, 2008.
- [22] K. Wang, E. Teoh, J. Jaros, and B. E. Treeby, "Modelling nonlinear ultrasound propagation in absorbing media using the k-Wave toolbox: Experimental validation," in *IEEE International Ultrasonics Symposium, IUS*, pp. 523–526, 2012.
- [23] F. A. Duck, *Physical properties of tissue : a comprehensive reference book*. London ;;San Diego: Academic Press, 1990.
- [24] M. F. Hamilton and D. T. Blackstock, *Nonlinear acoustics*. Academic Press, 1998.
- [25] T. Szabo, "Nonlinear Acoustics And Imaging," in *Diagnostic ultrasound imaging : inside out*, ch. 12, Elsevier Academic, 2004.
- [26] S. Butterworth, "On Electrically-maintained Vibrations," *Proceedings of the Physical Society of London*, vol. 27, pp. 410–424, 12 1914.
- [27] K. Van Dyke, "The Piezo-Electric Resonator and Its Equivalent Network," *Proceedings of the IRE*, vol. 16, pp. 742–764, 6 1928.
- [28] Wei-Gen Luo, Ai-Li Ding, Haosu Luo, and Zhi-Wen Yin, "High-field properties of PMN-PT single crystals," in *1999 IEEE Ultrasonics Symposium. Proceedings. International Symposium (Cat. No.99CH37027)*, vol. 2, pp. 1009–1012, IEEE, 1999.
- [29] S. Zhang and F. Li, "High performance ferroelectric relaxor-PbTiO 3 single crystals: Status and perspective," *Journal of Applied Physics*, vol. 111, p. 031301, 2 2012.
- [30] J. F. Blackburn and M. G. Cain, "Nonlinear piezoelectric resonance: A theoretically rigorous approach to constant I-V measurements," *J. Appl. Phys.*, vol. 100, p. 114101, 12 2006.



transducers.

Thong Huynh received a bachelor degree in Computer Engineering from HCMC University of technology, Vietnam and an M.Sc. degree in Micro and Nano system technology from the University College of Southeast Norway, Norway, in 2016. His master's thesis was Optimization of Ultrasound Pulses for Second Harmonic Imaging. He is currently pursuing the Ph.D. degree as an extension of his master thesis in the same department. His current main research interest is in theory, modeling and characterization of non ideal effects in ultrasound



Horten, Norway, where he is involved in the research and development in relation to cardiac ultrasound and with a main focus on electronics and processing for ultrasound data acquisition.

Geir Ultveit Haugen was born in 1965. He received the M.Sc. degree in electrical engineering and signal processing and the Ph.D. degree in geophysics from the Norwegian Institute of Technology, Trondheim, Norway, in 1989 and 1996, respectively. He was a Visiting Scientist at the Schlumberger Cambridge Research, Cambridge, U.K., in 2004. From 1996 to 2001, he was a Senior Geophysicist/Group Leader at the Statoil Research Center, Trondheim. He is a Senior Scientist/Group Leader of the Imaging and Acquisition team at GE Vingmed Ultrasound AS,



Currently, he is a member of the ultrasound probe R&D department at GE Vingmed Ultrasound. His interests are acoustics, array signal processing, and microelectronics.

Trym Eggen received the M.Sc. degree in electrical engineering from The Norwegian University of Science and Technology, Trondheim, Norway, and the Ph.D. degree from Massachusetts Institute of Technology, Cambridge, MA, USA, in 1989 and 1997, respectively. From 1989 to 2006, he was a Signal Processing Group Leader at Kongsberg Maritime, Horten, Norway, working on design of sonar and array systems. Since 2007, he has been with GE Vingmed Ultrasound, leading the development of 4D ultrasound TEE probes for cardiac imaging.



in 2008. His research interests include acoustics, ultrasound technology, and medical sensor technology in general. Since 2015, his main research is directed towards the 'Centre for Innovative Ultrasound Solutions', CIUS, where he is leader of the workpackage 'Transducers and Electronics'.

Lars Hoff received the M.Sc. degree in physics from the Norwegian Institute of Technology, NTH, Trondheim, Norway, in 1989, and the Ph.D. degree in acoustics from the Norwegian University of Science and Technology, NTNU, Trondheim, in 2000. During most of the 1990s, he worked on contrast agents for medical ultrasound imaging, first with the company Nycomed Imaging AS, later with NTNU. In 2003, he started working at Vestfold University College, today merged into the University South-Eastern Norway, where he was appointed professor